GEOPHYSICS, VOL. 86, NO. 1 (JANUARY-FEBRUARY 2021); P. E21–E35, 11 FIGS., 2 TABLES.
10.1190/GEO2018-0792.1

Check for updates

Downloaded 01/04/21 to 130.54.110.22. Redistribution subject to SEG license or copyright; see Terms of Use at https://library.seg.org/page/policies/terms
DOI:10.1190/geo2018-0792.1

Method for obtaining response functions from noisy magnetotelluric data using frequency-domain independent component analysis

Shinya Sato[1], Tada-Nori Goto[2], Takafumi Kasaya[3], and Hiroshi Ichihara[4]

ABSTRACT

The magnetotelluric (MT) method has been used for visualizing subsurface resistivity structures and more recently for monitoring resistivity changes. However, electromagnetic data often include cultural noise, which can cause errors in the estimation of MT response functions and subsurface resistivity structure analysis. Frequency-domain independent component analysis (FDICA) offers advantages for MT data processing particularly because this method can extract hidden components in the observed data. These components can be decomposed into natural MT signals and cultural noise so that the noise effect in the recovered MT data is reduced. FDICA is applied to MT data acquired at the Kakioka Magnetic Observatory in Japan. The apparent resistivity and phase curves are obtained with small estimated errors between periods of 7 and 12,000 s, although the length of the time-series data is limited. The curves are smoother than those obtained using a conventional method. Various types of synthetic noise are added to the time series at Kakioka to test the noise-reduction performance of FDICA for MT data with high noise contamination. The results demonstrate that FDICA can be used to estimate MT response functions with high accuracy even under conditions in which more than half of the time-series data are contaminated by noise.

INTRODUCTION

Magnetotellurics (MT) is an electromagnetic (EM) exploration method that can visualize deep subsurface resistivity structures. Time-lapse MT sounding has recently been conducted to monitor the subsurface resistivity structure around volcanic regions as potential geothermal energy sources (Aizawa et al., 2011; Peacock et al., 2013) and gas reservoirs (He et al., 2015; Rees et al., 2016). The temporal changes in apparent resistivity and phase (MT response functions) are generally small (e.g., 20% of the apparent resistivity changes reported by Aizawa et al., 2011). However, the accuracy of MT measurements is often degraded by artificial (cultural) noise mixed in the electric and magnetic data (referred to as MT data in this study). Cultural noise from power lines, direct current (DC) electric railways, sensor vibration, and other sources can cause large errors in the estimated response functions (Szarka, 1988; Junge, 1996). The detection of temporal changes is therefore difficult if the degree of changes is within the range of the estimated errors.

Substantial research efforts have addressed the processing of MT data contaminated by cultural noise. Vozoff (1972) proposes a simple stacking of spectra, and Gamble et al. (1979a) develop remote-reference processing to reduce the bias on MT responses owing to local noise. Combined robust estimation and remote-reference processing (Egbert and Booker, 1986; Chave et al., 1987) were then proposed as well as a modified method involving a bound on the influence of the magnetic field (Chave and Thomson, 2004). Robust remote references with principle component analysis have also been reported for MT array data (Egbert, 1997; Egbert, 2002; Smirnov and Egbert, 2012) and can offer more robustness to noisy data than the previous methods when array data are available. Other approaches have also been presented in the literature: Weckmann et al. (2005) derive a manual scheme to find and mask

Partly presented at the 87th Annual Meeting on 27 September 2017. Manuscript received by the Editor 28 November 2018; revised manuscript received 12 July 2020; published ahead of production 30 September 2020; published online 30 December 2021.
[1]Kyoto University, Graduate School of Engineering, Kyoto 615-8540, Japan. E-mail: shinya.sato.27s@st.kyoto-u.ac.jp (corresponding author).
[2]University of Hyogo, Graduate School of Life Science, Hyogo 671-2280, Japan. E-mail: t.n.goto@sci.u-hyogo.ac.jp.
[3]Japan Agency for Marine-Earth Science and Technology, Kanagawa 237-0061, Japan. E-mail: tkasa@jamstec.go.jp.
[4]Nagoya University, Graduate School of Environmental Studies, Aichi 464-8603, Japan. E-mail: h-ichi@seis.nagoya-u.ac.jp.
© 2021 Society of Exploration Geophysicists. All rights reserved.

Downloaded 01/04/21 to 130.54.110.22. Redistribution subject to SEG license or copyright; see Terms of Use at https://library.seg.org/page/policies/terms
DOI:10.1190/geo2018-0792.1

noise spectra, Neukirch and Garcia (2014) propose a method to handle nonstationary noise, and Chave (2017) builds a new statistical model for the estimation of MT responses. These methods have been widely used and can be applied to obtain highly accurate MT response estimates. However, cases in which cultural noise still contaminates substantial portions of the time series may result in a very low signal-to-noise (S/N) ratio of the data and possibly low-quality MT responses.

Time-domain independent component analysis (TDICA) has been recently applied to extract signals in various geophysical fields (Ikelle, 2007; Tsuno and Iwata, 2015; Imamura et al., 2017; Sato et al., 2017). This method was originally developed to decompose observed multichannel data (e.g., audio data) into independent and separated components (Hyvärinen et al., 2001). The application of TDICA to decompose MT signals and noise from observed data has also been proposed (Cui et al., 2013; Mizunaga, 2016). In the time domain, however, phase differences between the electric and magnetic fields owing to induction phenomena must be considered. The performance of TDICA degrades when processing MT data because they require no phase shift in the observed data (Hyvärinen et al., 2001). To overcome this problem, we use the method of frequency-domain independent component analysis (FDICA), which was originally introduced by Smaragdis (1998) for blind source separation. FDICA extends TDICA to the complex domain, which is applicable to the temporal changes of complex spectra. FDICA accommodates data with phase differences in the time domain, such as MT data. However, some challenges remain when applying conventional FDICA to MT data, as discussed later. To lessen these problems, we attach four processes and develop a new processing code for MT data using FDICA (i.e., an MT processing scheme based on FDICA, or shortened as FDICA-MT) to reduce cultural noise that contaminates substantial portions of the local time series.

In this work, the performance of FDICA-MT is tested on data acquired at the Kakioka Magnetic Observatory, Japan. The results are compared with the popular tool bounded influence remote reference processing (BIRRP) (Chave and Thomson, 2004) to verify the accuracy and reliability of FDICA-MT. We illustrate the noise-reduction performance of FDICA-MT by adding various levels of synthetic noise to the raw data, and impedances are successfully recovered even under considerable noise contamination. We use the term "source signals" in the mathematical introduction of FDICA, which means unmixed/original components (e.g., MT signals and noise), and the terms "MT signals" and "noise" directly to discuss the detailed FDICA-MT processes.

FDICA

Theory of FDICA

FDICA was originally introduced by Smaragdis (1998) to decompose observed data into separated components in the time-frequency domain after applying the short-time Fourier transform (STFT). Consider that FDICA is applied to the observed data with four channels. The observed data $\boldsymbol{X}(f,\tau) = \{X_1(f,\tau), \ldots, X_4(f,\tau)\}^{\mathrm{tr}}$, which is a transpose matrix of $\{X_1(f,\tau), \ldots, X_4(f,\tau)\}$ at a frequency f and with T time windows ($\tau = 1, \ldots, T$), are assumed to be linear combinations of four independent source signals $\boldsymbol{S}(f,\tau) = \{S_1(f,\tau), \ldots, S_4(f,\tau)\}^{\mathrm{tr}}$. If the total number of source signals is equal to the number of observed data (i.e., four), the following equation can be expressed with a mixing matrix $\boldsymbol{A}(f)$ (4×4 matrix):

$$\boldsymbol{X}(f,\tau) = \boldsymbol{A}(f)\boldsymbol{S}(f,\tau). \tag{1}$$

Using FDICA, separated components $\boldsymbol{Y}(f,\tau) = \{Y_1(f,\tau), \ldots, Y_4(f,\tau)\}^{\mathrm{tr}}$ are obtainable at each frequency and for each time window. The separation matrix $\boldsymbol{W}(f)$ is also obtainable at each frequency:

$$\boldsymbol{Y}(f,\tau) = \boldsymbol{W}(f)\boldsymbol{X}(f,\tau). \tag{2}$$

Each separated component is an estimated source signal, and the inverse separation matrix $\boldsymbol{W}^{-1}$ is an estimated mixing matrix $\boldsymbol{A}$ and denotes the contributions of each $\boldsymbol{Y}$ to $\boldsymbol{X}$. However, the separated components do not always have the same index number as the corresponding source signals. For example, Y_1 does not always correspond to S_1, but it may, for instance, correspond to S_2 instead. Additionally, separated components $\boldsymbol{Y}$ do not always have the same phases and powers as $\boldsymbol{S}$. The correspondence between the separated components and the source signals and recovery of phases and powers must be determined based on $\boldsymbol{W}^{-1}(f)$.

Two conditions are required for extracting $\boldsymbol{Y}$ with high accuracy: Source signals must be mutually independent, and the source signals' distributions must not be Gaussian. When several source signals $\boldsymbol{S}$ mix, the observed data $\boldsymbol{X}$ follow a Gaussian distribution by the central limit theorem, so we assume in FDICA that $\boldsymbol{S}$ (i.e., before mixing) follows a non-Gaussian distribution (Amari et al., 1996; Hyvärinen and Oja, 2000; Hyvärinen et al., 2001).

Let us consider that the observed data are MT data and the source signals correspond to two polarized MT signals and noise components. As reported in Vörös et al. (1998), the empirical probability density function (PDF) of MT signals (i.e., the geomagnetic fluctuations) frequently has a long tail, which is not easily modeled by a Gaussian distribution. Cultural noise also often has large amplitudes, which implies that its PDF also has a long tail. We thus model the separated components corresponding to source signals (i.e., MT signals and noise) by a Laplace distribution because it has a longer tail than a Gaussian distribution.

Following conventional FDICA (Murata and Ikeda, 1998), we use "mutual information" as an indicator of statistical independence, a measure of the information that members of a set of random variables have on other random variables in the set and is defined by equation 5.17 in Hyvärinen et al. (2001). In FDICA based on mutual information, the separation matrix $\boldsymbol{W}(f)$ can be optimized to satisfy the independence between each pair of separated components following the algorithm by Murata and Ikeda (1998; equation 9):

$$\begin{aligned}\boldsymbol{W}^{t+1}(f) = \boldsymbol{W}^{t}(f) + \alpha(\mathrm{diag}[\mathrm{EV}[\varphi(\boldsymbol{Y}(f,\tau))\boldsymbol{Y}(f,\tau)^{H}]] \\ - \mathrm{EV}[\varphi(\boldsymbol{Y}(f,\tau))\boldsymbol{Y}(f,\tau)^{H}])\boldsymbol{W}^{t}(f),\end{aligned} \tag{3}$$

where EV denotes the expected value, superscript H represents the Hermitian transpose of $\boldsymbol{Y}(f,\tau)$, and t indicates the current iteration. Additionally, $\varphi(\boldsymbol{Y})$ represents the activation function defined as $\varphi(\boldsymbol{Y}) = \tanh(\eta \cdot \mathrm{Re}\{\boldsymbol{Y}\}) + j \cdot \tanh(\eta \cdot \mathrm{Im}\{\boldsymbol{Y}\})$, where j denotes the imaginary unit and can be obtained by modeling $\boldsymbol{Y}$ as a Laplace distribution according to Murata and Ikeda (1998) and Hyvärinen

Downloaded 01/04/21 to 130.54.110.22. Redistribution subject to SEG license or copyright; see Terms of Use at https://library.seg.org/page/policies/terms
DOI:10.1190/geo2018-0792.1

et al. (2001). We use $\eta = 100$ following Mukai et al. (2003) and Sawada et al. (2003) to stabilize the gradient defined by the activation function $\varphi(\boldsymbol{Y})$. In equation 3, α is a step coefficient related to the convergence speed of the iteration and has a value of 0.1 because Mukai et al. (2003) and Sawada et al. (2004) demonstrate the stability of convergence with such a value. The initial value of $\boldsymbol{W}(f)$ is set as the identity matrix because its convergence is faster than set as a random matrix (Tachibana et al., 2007).

When handling small amplitude data, the gradient defined by the second term on the right side of equation 3 can become unstable because $\varphi(\boldsymbol{Y})$ approaches zero. To prevent this, the scale of the observed data $\boldsymbol{X}(f,\tau)$ should be normalized. We multiply $\boldsymbol{X}(f,\tau)$ by the scaling matrix $\boldsymbol{Q}(f)$, which denotes the reciprocal of the average power of squared spectra, before applying FDICA:

$$\boldsymbol{Q}(f) = \sqrt{\mathrm{diag}\left(\frac{T}{\sum_{\tau}\boldsymbol{X}(f,\tau)\boldsymbol{X}(f,\tau)^{H}}\right)}, \tag{4}$$

where T is the total number of time windows, as mentioned above. Our study defines the inverse separation matrix including $\boldsymbol{Q}(f)$ as

$$\boldsymbol{B}(f) = (\boldsymbol{W}(f)\boldsymbol{Q}(f))^{-1}. \tag{5}$$

Example of blind source separation with conventional FDICA

A simple example of conventional FDICA processing is portrayed in Figure 1, which demonstrates how conventional FDICA can extract separated components from only the observed data. Two source signals (Figure 1a), which are combinations of random noise and small rectangular waves with a length of 12,736 s, are assumed to be independent in the time domain. The number of observed data is also assumed to be two (Figure 1b), which are composed of two source signals with phase differences of 1 s and mixing matrix $\boldsymbol{A} = \begin{pmatrix} 1 & 0.5 \\ 0.5 & -1 \end{pmatrix}$. After applying FDICA with a Fourier transform length of 128, 256, and 512 s, and processing by inverse STFT, we decompose the data into two separated components (the right two graphs in Figure 1). In the time domain, two independent components are extracted: Separated component 1 corresponds to source signal 1, and separated component 2 corresponds to source signal 2, although the sign is reversed. However, the source signals' amplitudes, signs, or phases recorded in the observed data can be reconstructed using the inverse separation matrix $\boldsymbol{B}(f)$ in equation 5 because it denotes the contributions of the separated components to the observed data.

Performance of conventional FDICA under some inherent noise

Conventional FDICA requires that the total number of source-signal components is the same as the number of observed components. However, this assumption might not hold for actual MT observations. For example, the time-series data at an MT site may be contaminated by several cultural noise sources such as power generators, factories, and DC railways. Sawada et al. (2006) report that FDICA can estimate only large source signals from the observed data, including several source signals in such cases.

By focusing on a frequency f, we confirm the ability of signal extraction by FDICA based on eight signals mixed as

$$\begin{pmatrix} X_1(f,\tau) \\ X_2(f,\tau) \\ X_3(f,\tau) \\ X_4(f,\tau) \end{pmatrix} = \begin{pmatrix} \boldsymbol{I}_2 & \boldsymbol{I}_2 \\ \boldsymbol{0} & \boldsymbol{I}_2 \end{pmatrix} \begin{pmatrix} N_x(f,\tau) \\ N_y(f,\tau) \\ S_x(f,\tau) \\ S_y(f,\tau) \end{pmatrix} + a\boldsymbol{I}_4 \begin{pmatrix} N_1(f,\tau) \\ N_2(f,\tau) \\ N_3(f,\tau) \\ N_4(f,\tau) \end{pmatrix}, \tag{6}$$

where $\boldsymbol{I}_K$ is the identity matrix ($K \times K$ matrix) and $X_1, \ldots, X_4$ are four observed data. The terms S_x, S_y, N_x, and N_y are four synthetic independent source signals, which are spectra based on rectangular waves in the time-frequency domain, are normalized, and have 80 time windows. In a more realistic case, S_x and S_y can be considered as natural MT signals that randomly fluctuate and N_x and N_y correspond to cultural noise components. Additionally, $N_1, \ldots, N_4$ are considered random-Gaussian inherent noise components, which create an undesired condition for FDICA.

By varying the inherent noise coefficient (a) from 0 to 1, we apply FDICA to the four observed data and extract the separated components and inverse separation matrix $\boldsymbol{B}$ (equation 5). We can estimate the reciprocal S/N of $X_i (i = 3, 4)$ using

$$\mathrm{Est}_{\mathrm{NS}}(X_i(f,\tau)) = \frac{\sum |B_{\text{noise in } X_i}|}{\sum |B_{\text{signal in } X_i}|}, \tag{7}$$

where $B_{\text{noise in } X_i}$ and $B_{\text{signal in } X_i}$ are elements of $\boldsymbol{B}$ and denote the contribution of the noise components to X_i and those of the MT signal components, respectively. Therefore, the ratio of the summation of $|B_{\text{noise in } X_i}|$ over that of $|B_{\text{signal in } X_i}|$ denotes the reciprocal S/N of X_i based on the FDICA results. Because no noise is included in X_3 and X_4, $\mathrm{Est}_{\mathrm{NS}}$ originally indicates zero. If the inherent noise becomes large, then $\mathrm{Est}_{\mathrm{NS}}$ increases owing to the substantial degradation of the separation performance. Additionally, considering X_3 and X_4 as inputs and X_1 and X_2 as outputs, we define here the simple response function (SRF) as

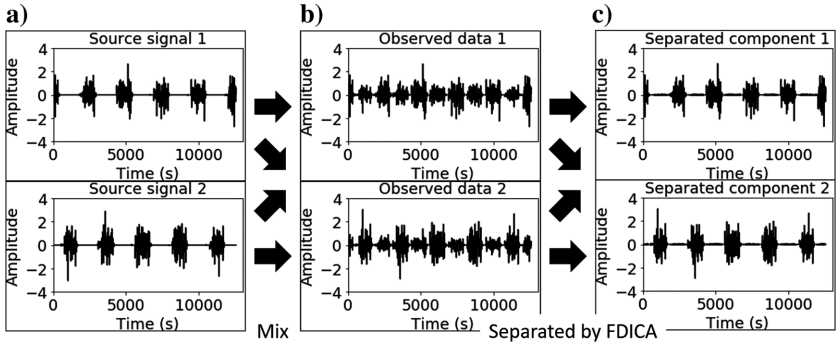

Figure 1. Example of FDICA processing. (a) Two independent source signals in the time domain. (b) Observed data with two channels with phase shifting. (c) Two separated components obtained from FDICA.

Downloaded 01/04/21 to 130.54.110.22. Redistribution subject to SEG license or copyright; see Terms of Use at https://library.seg.org/page/policies/terms
DOI:10.1190/geo2018-0792.1

$$\mathrm{SRF}(f) = \frac{1}{2}\left(\frac{\sum |B_{\text{signal in } X_1}|}{\sum |B_{\text{signal in } X_3}|} + \frac{\sum |B_{\text{signal in } X_2}|}{\sum |B_{\text{signal in } X_4}|}\right). \quad (8)$$

SRF indicates an initial value of one because of equation 6, and it changes when the inherent noise is included in the signal components. After 10,000 trials with randomization, the average $\mathrm{Est_{NS}}$ and SRF are calculated, as presented in Table 1. The results show that the SRF deviates largely from one when the $\mathrm{Est_{NS}}$ surpasses 0.1–0.2 (i.e., $a > 0.2$–0.5). As shown in Table 1 and reported in Sawada et al. (2006), we can extract the natural MT signals and large noise exactly using FDICA if the additional inherent noise has small amplitudes.

MT PROCESSING SCHEME BASED ON FDICA (FDICA-MT)

Using FDICA, we fundamentally decompose the four observed components as (1) two horizontal magnetic-field and electric-field data, (2) two electric-field and two reference data, or (3) two horizontal magnetic-field and two reference data. FDICA enables decomposition of the observed data into two-polarized MT signals and two unknown cultural noise components under the condition that the sources of the two-polarized signals (e.g., the north–south and east–west directions) and the sources of the two noise components are independent and follow Laplace distributions. Although Chave (2017) shows that MT data are systematically long-tailed and can be described by a stable distribution family, FDICA has only as yet been specifically defined for the long-tailed Laplace distribution, as mentioned previously. However, the critical point is that FDICA optimizes the signal non-Gaussianity, which is a common characteristic between the two distributions. Two noise factors may be correlated accidentally because of large-amplitude cultural noise during the daytime. In this case, FDICA estimates only EM signals exactly if the independence between EM signals and noise holds.

Conventional FDICA involves two important difficulties for MT data analysis: (1) It is difficult to determine whether the separated components represent MT signals or noise (a "permutation problem") and (2) the signal-separation performance of FDICA is imperfect ("limited ability of signal separation"). For the first problem, we must distinguish the correspondence of each separated component to one source signal at each frequency. As shown in Figure 1, matching of the true source signals and separated components is not achieved. The second problem is caused by a severe noise environment, where most of the time-series MT data are contaminated by cultural noise. The noise's waveform can spuriously correlate with the MT signals' waveforms, although their sources are independent. Moreover, as shown in Table 1 and Sawada et al. (2006), if the total number of MT signals and cultural/inherent noise components is larger than four, the estimation of the separated components degrades. We therefore present solutions to the permutation problem and the limited ability of signal separation. We use the S/N of local magnetic-field data to provide a solution to the permutation problem. Subsequently, we propose a solution to the limited ability of signal separation in which we select data sections with small inherent noise determined by FDICA at each frequency.

This study develops a new scheme for MT analysis, improving the conventional FDICA, and it proposes an outline of FDICA-MT. Cores of the algorithm designated as FDICA-MT are summarized in Figure 2, where the processes of **PA**, **PB**, **PC**, and **PD** are newly proposed in this study. The observed data are transformed by STFT using a Hamming window. The entire time-dependent spectra are divided into L data sections. For example, $E_x(f,\tau)$ is divided into $E_x(f,l,\tau_l)$, $(l = 1, \ldots, L$ and $\tau_l = 1, \ldots, T_L)$, where $T_L = T/L$. We define the number of data sections L satisfying the condition that each section length T_L is longer than 100 to avoid very short data lengths, which possibly cause the accidental correlation of independent waveforms. In the case of analysis of a long period, L should be small due to the limited time-series data and longer Fourier transform length. We derive the separated components $\boldsymbol{Y}(f,l,\tau_l)$ and inverse separation matrix $\boldsymbol{B}(f,l)$ at each frequency f and each data section l.

S/N ratio estimation of local magnetic-field data

As important parameters in our algorithm (**PA** in Figure 2), we propose minimum values of the S/N of local magnetic-field data: $m_{\mathrm{SN}}(d,f,l)$ for d component $(d = x, y)$. Here, we focus on the x-direction of the magnetic field at one frequency in one data section and omit its section ID (l). Using the Gram-Schmidt orthonormalization, the time-dependent complex spectra of local magnetic-field data $\boldsymbol{H}_x(f) = \{H_x(f,1), \ldots, H_x(f,T)\}^{\mathrm{tr}}$, which is a vector notation of $H_x(f,\tau)(\tau = 1, \ldots, T)$, can be decomposed into a correlated part with the reference magnetic-field data $\boldsymbol{R}_x(f) = \{R_x(f,1), \ldots, R_x(f,T)\}^{\mathrm{tr}}$ and an uncorrelated part:

$$\boldsymbol{H}_x(f) = \left\{\frac{\langle \boldsymbol{R}_x^*(f), \boldsymbol{H}_x(f)\rangle}{\langle \boldsymbol{R}_x^*(f), \boldsymbol{R}_x(f)\rangle}\boldsymbol{R}_x(f)\right\} + \left\{\boldsymbol{H}_x(f) - \frac{\langle \boldsymbol{R}_x^*(f), \boldsymbol{H}_x(f)\rangle}{\langle \boldsymbol{R}_x^*(f), \boldsymbol{R}_x(f)\rangle}\boldsymbol{R}_x(f)\right\}. \quad (9)$$

Here, superscript $*$ indicates the conjugate vector of $\boldsymbol{R}_x$ and "$\langle \boldsymbol{R}_x^*, \boldsymbol{H}_x\rangle$" denotes the inner product of $\boldsymbol{R}_x^*$ and $\boldsymbol{H}_x$. The first term on the right side of equation 9 is the correlated part of $\boldsymbol{H}_x$ with $\boldsymbol{R}_x$, and the second is the uncorrelated part. Reference data used in FDICA-MT are assumed to include no noise that correlates with

Table 1. The summation of $\mathrm{Est_{NS}}$ in equation 7 and SRF in equation 8.

a	0	0.1	0.2	0.3	0.4	0.5	0.6	0.7	0.8	0.9	1
$\mathrm{Est_{NS}}(X_3)$	0.01	0.04	0.09	0.14	0.20	0.25	0.30	0.33	0.36	0.39	0.41
$\mathrm{Est_{NS}}(X_4)$	0.01	0.04	0.09	0.14	0.20	0.25	0.30	0.33	0.37	0.39	0.41
SRF	0.97	0.99	0.97	0.95	0.92	0.89	0.85	0.79	0.74	0.69	0.66

Note: The row labeled "a" indicates the amplitudes of the inherent noise.

Downloaded 01/04/21 to 130.54.110.22. Redistribution subject to SEG license or copyright; see Terms of Use at https://library.seg.org/page/policies/terms
DOI:10.1190/geo2018-0792.1

the local noise. Dividing the Euclidean norm of the correlated part in equation 9 by that of the uncorrelated part, we obtain $m_{\mathrm{SN}}(x,f)$ defined as

$$m_{\mathrm{SN}}(x,f)=\frac{\left|\frac{\langle \boldsymbol{R}_x^*(f),\boldsymbol{H}_x(f)\rangle}{\langle \boldsymbol{R}_x^*(f),\boldsymbol{R}_x(f)\rangle}\boldsymbol{R}_x(f)\right|}{\left|\boldsymbol{H}_x(f)-\frac{\langle \boldsymbol{R}_x^*(f),\boldsymbol{H}_x(f)\rangle}{\langle \boldsymbol{R}_x^*(f),\boldsymbol{R}_x(f)\rangle}\boldsymbol{R}_x(f)\right|}, \qquad (10)$$

which is smaller than the squared "true" S/N of $\boldsymbol{H}_x$ as described in Appendix A. Although it is not realistic, $m_{\mathrm{SN}}(x,f)$ is equal to the true S/N when the noise at the reference site is zero. Nevertheless, we ascertain that $m_{\mathrm{SN}}(x,f)$ and $m_{\mathrm{SN}}(y,f)$ represent the minimum values of S/N of the local magnetic-field data.

Determination of MT signals and noise from separated components

Here, we focus on one data section, omit its section ID (l), and focus on a frequency f. If $m_{\mathrm{SN}}(x,f)\geq 1$ and $m_{\mathrm{SN}}(y,f)\geq 1$, the local MT data are decomposed into four separated components using FDICA. When the number of MT signals is limited to two as reported in Egbert (2002), the two polarized signals may be determined based on the maximum contribution to the magnetic field data.

However, Sawada et al. (2006) and Hiroe (2009) report that one or more meaningless separated components can be generated when the total number of MT signals and noise components (aside from small or inherent noise) is less than four. Because such components include MT signals or noise components due to the limited ability of signal separation, as discussed later, it might be more appropriate that one signal or noise component is represented by two or more separated components. To accommodate this case, the determination is based on the inverse separation matrix $\boldsymbol{B}(f)$ in equation 5 by the evaluation of $m_{\mathrm{SN}}(x,f)$ and $m_{\mathrm{SN}}(y,f)$ (**PB1** in Figure 2). For example, we consider that the MT signal components derived from the x-direction magnetic field are determined. We then search all $B_{3k}(f)$ that satisfy

$$|B_{3k}(f)|\geq\frac{1}{\lambda_{\min}}\max_k|B_{3k}(f)| \times(\lambda_{\max}>m_{\mathrm{SN}}(x,f)\geq\lambda_{\min}). \qquad (11)$$

All $Y_k(k=1,\ldots,4)$ corresponding to $B_{3k}(f)$ that satisfy equation 11 are considered as MT signal components. The function $\max_k B_{3k}(f)$ denotes the maximum value in the contribution of the separated components $Y_k(f,\tau)$ to the x-direction magnetic-field data. The two variables $\lambda_{\max}$ and $\lambda_{\min}$ are thresholds for distinguishing the MT signal and noise components and are set by three steps: (1) $(\lambda_{\max},\lambda_{\min})=(+\infty,10)$, (2) $(\lambda_{\max},\lambda_{\min})=(10,\sqrt{10})$, and (3) $(\lambda_{\max},\lambda_{\min})=(\sqrt{10},1)$. The relationship between the m_{SN} (or the true S/N) and FDICA results (i.e., B) cannot be derived exactly because it depends on the data conditions. Thus, from the experience of our numerical tests in changing the true S/N and deriving m_{SN}, we set the pairs of thresholds $(\lambda_{\max},\lambda_{\min})$ in equation 11 as above, although they can be set differently by other users. The reason for a stepped threshold rather than a continuous threshold is explained in Appendix B. To determine the MT signal components corresponding to the y-direction magnetic field, $B_{3k}(f)$ and $m_{\mathrm{SN}}(x,f)$ are replaced by $B_{4k}(f)$ and $m_{\mathrm{SN}}(y,f)$. The other separated components are regarded as noise components.

At a frequency where $m_{\mathrm{SN}}(x,f)<1$ or $m_{\mathrm{SN}}(y,f)<1$, we cannot reliably consider the separated components with high contributions to the local data as MT signals (i.e., the MT signals cannot be determined following equation 11). In such a case, FDICA is applied

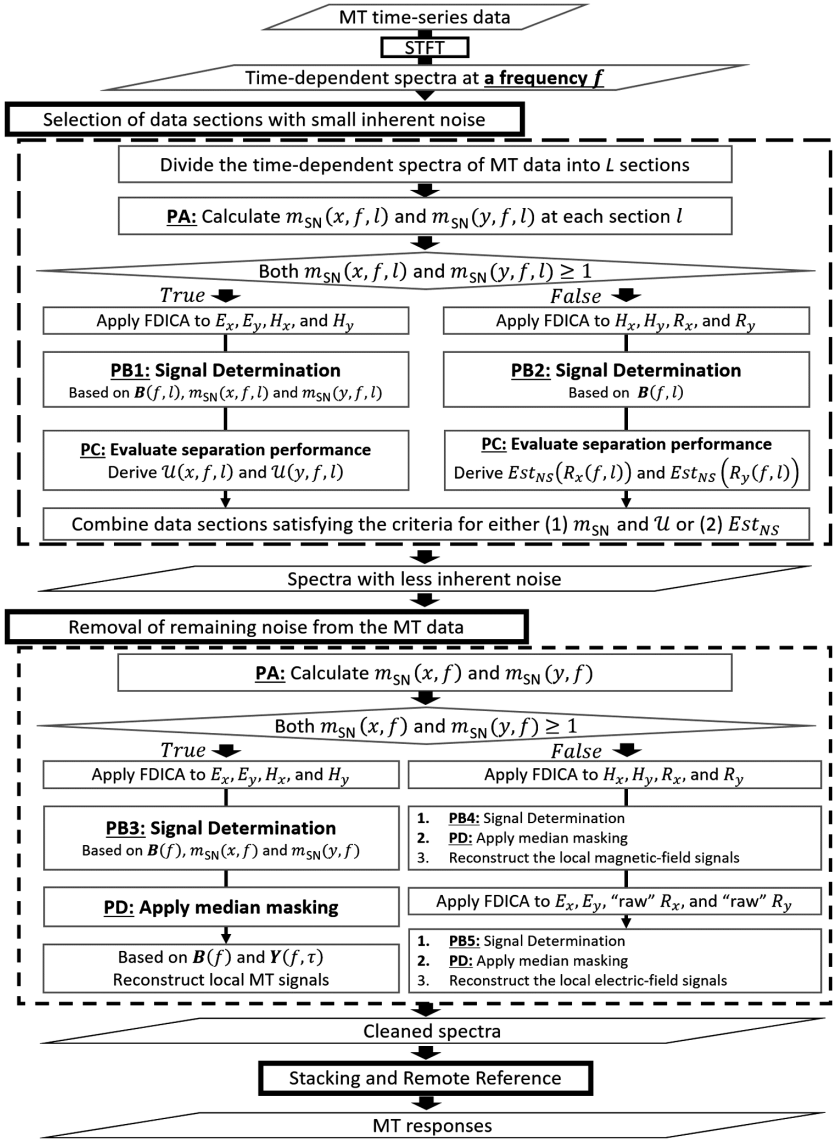

Figure 2. FDICA-MT analysis flow. The symbols $\mathrm{Est}_{\mathrm{NS}}$, m_{SN}, and $\mathcal{U}$ are defined by equations 7, 10, and 13, respectively. The processes in bold are newly adopted to conventional FDICA.

Downloaded 01/04/21 to 130.54.110.22. Redistribution subject to SEG license or copyright; see Terms of Use at https://library.seg.org/page/policies/terms
DOI:10.1190/geo2018-0792.1

to the two local magnetic-field data and two reference data (see the upper "decision" symbol in Figure 2) assuming that the reference data have sufficiently high S/Ns and there exist two polarized signals, as reported in Egbert (2002). Let us consider that H_x, H_y, R_x, and R_y are the magnetic-field data at the local and reference sites, S_x and S_y are the natural MT signals, N_x and N_y represent the local noise, $\boldsymbol{T_L}$ and $\boldsymbol{T_R}$ denote the mixing matrix of the MT signals, and $\boldsymbol{A_n}$ represents the mixing matrix of the noise. The ideal condition of the local and reference data can be represented as

$$\begin{pmatrix} H_x(f,\tau) \\ H_y(,\tau) \\ R_x(f,\tau) \\ R_y(f,\tau) \end{pmatrix} = \begin{pmatrix} \boldsymbol{A_n}(f) & \boldsymbol{T_L}(f) \\ \boldsymbol{0} & \boldsymbol{T_R}(f) \end{pmatrix} \begin{pmatrix} N_x(f,\tau) \\ N_y(f,\tau) \\ S_x(f,\tau) \\ S_y(f,\tau) \end{pmatrix}. \quad (12)$$

Based on equation 12, only two separated components with a maximum value in the contribution to the reference data are then regarded as MT signals (**PB2** in Figure 2).

Selection of data sections with small inherent noise

For a good signal-separation performance of FDICA, we propose a method to select the data sections with small inherent noise (**PC** in Figure 2). At a data section or frequency with $m_{\mathrm{SN}}(x,f,l) \geq 1$ and $m_{\mathrm{SN}}(y,f,l) \geq 1$, after the signal determination based on equation 11, we can estimate the reciprocal of S/N (i.e., N/S) of magnetic-field data using $\mathrm{Est_{NS}}$ in equation 7, whose X_k is replaced by $H_{xory}(f,l)$. Although m_{SN} is only dependent on S/N, $\mathrm{Est_{NS}}$ is dependent on S/N and the signal-separation performance of FDICA. We therefore assume that each reciprocal of $\mathrm{Est_{NS}}(H_x(f,l))$ and $\mathrm{Est_{NS}}(H_y(f,l))$ should be far from $m_{\mathrm{SN}}(x,f,l)$ and $m_{\mathrm{SN}}(y,f,l)$ in the presence of large inherent noise when the signal separation degrades. The product of $\mathrm{Est_{NS}}$ and m_{SN},

$$\mathcal{U}(d,f,l) = \mathrm{Est_{NS}}(H_d(f,l)) \cdot m_{\mathrm{SN}}(d,f,l)(d = x,y), \quad (13)$$

indicates the signal-separation performance and is used to identify data sections with small inherent noise. We assume the data sections, where each $\mathcal{U}(x,f,l)$ and $\mathcal{U}(y,f,l)$ has a value larger than a threshold, to be less contaminated by inherent noise. Because $\mathcal{U}$ in equation 13 can become small by the bias effect of m_{SN}, setting a large threshold would possibly lead to the rejection of many data sections in which FDICA works well. We set a small threshold between 0.06 and 0.10, and we tested various values and obtained stable results within this range. Although this value can be set by users, in real data analysis, we recommend a threshold of 0.1. Furthermore, we assume that the data with m_{SN} higher than $\sqrt{10}$ are less contaminated and $\mathcal{U}(d,f,l)$ is derived only if any $m_{\mathrm{SN}}(d,f,l)$ is between 1 and $\sqrt{10}$.

At a data section or frequency with $m_{\mathrm{SN}}(x,f,l) < 1$ or $m_{\mathrm{SN}}(y,f,l) < 1$, after applying FDICA to the two local magnetic-field data and two reference data, we evaluate the signal-separation performance at each section using $\mathrm{Est_{NS}}$ in equation 7, whose X_k is replaced by $R_x(f,l)$ or $R_y(f,l)$ (see **PC** at the top right in the flowchart, Figure 2). The $\mathrm{Est_{NS}}(R_x(f,l))$ and $\mathrm{Est_{NS}}(R_y(f,l))$ indicate zeros under no inherent noise conditions in the reference data because the latter are assumed to include no noise that correlates to local noise. According to the results in Table 1, $\mathrm{Est_{NS}}$ should not exceed 0.1–0.2. In real data analysis, data sections with $\mathrm{Est_{NS}}$ values less than 0.1 are regarded to contain a sufficiently strong signal (i.e., low inherent noise) and are further considered.

After selecting the data sections with small inherent noise, these divided sections are combined into $H_x(f,\tau)$, $H_y(f,\tau)$, $E_x(f,\tau)$, and $E_y(f,\tau)$, where τ is renumbered from 1 to $T_s(f)$ ($T_s(f)$ is the total number of spectra in the selected data sections at a frequency f). As a result, we can obtain the temporal changes of complex spectra that are less affected by inherent noise that cannot be extracted using FDICA. However, large coherent noise might remain in the temporal changes of complex spectra, which may still be removed using FDICA.

Removal of remaining noise from the MT data

We recalculate m_{SN} from the above obtained MT spectra. We then propose two analytical flows in the cases of (1) $m_{\mathrm{SN}}(x,f)$ and $m_{\mathrm{SN}}(y,f) \geq 1$ and (2) $m_{\mathrm{SN}}(x,f)$ or $m_{\mathrm{SN}}(y,f) < 1$ (the lower decision symbol in the flowchart, Figure 2).

When both m_{SN} are equal to or greater than one, FDICA is applied to the four local MT data and the four separated components can be obtained. Following equation 11, the four separated components are assigned to natural MT signals or noise (**PB3** in Figure 2, the same as **PB1**). However, the separated noise components, $Y_{\mathrm{noise}}(f,\tau)$, may still include a part of the MT signal components. The large amplitudes of $Y_{\mathrm{noise}}(f,\tau)$ strongly affect the low S/N and should be treated as noise components. For removing only the large amplitudes of $Y_{\mathrm{noise}}(f,\tau)$ from the MT analysis (**PD** in Figure 2), we apply median masking to $Y_{\mathrm{noise}}(f,\tau)$:

$$Y_{\mathrm{noise}}(f,\tau) = \begin{cases} 0 & (|Y_{\mathrm{noise}}(f,\tau)| \geq |Y_{\mathrm{noise,med}}(f)|) \\ Y_{\mathrm{noise}}(f,\tau) & (|Y_{\mathrm{noise}}(f,\tau)| < |Y_{\mathrm{noise,med}}(f)|) \end{cases}, \quad (14)$$

where $|Y_{\mathrm{noise,med}}(f)|$ is the median value of $|Y_{\mathrm{noise}}(f,\tau)|(\tau = 1, \ldots, T_s(f))$. Sawada et al. (2006) test that masking more amplitudes from the separated components can lead to a loss of more target signals, and less masking leads to an increase of the remaining noise. We thus set the threshold to the median. The remaining spectra after applying median masking are recognized as MT signals. The MT data can be reconstructed from the inverse separation matrix $\boldsymbol{B}(f)$ and unmasked/masked separated components $\boldsymbol{Y}(f,\tau)$. Even in the case in which the remaining spectra are noise, their effects on the S/N of the MT data are smaller than the effect of the masked (large) amplitudes. The number of spectra is not reduced because not the time windows but only the amplitudes of $Y_{\mathrm{noise}}(f,\tau)$ are removed. This advantage denotes that FDICA-MT directly removes noise from only the local data.

If either m_{SN} is less than one, FDICA is applied to the two local magnetic-field data and two reference data. In the obtained four separated components, the noise and natural MT signals are determined on the basis of $\boldsymbol{B}(f)$ (**PB4** in Figure 2, the same process as **PB2**). As above, the median masking in equation 14 is applied to the separated components regarded as noise (**PD** in Figure 2). Using $\boldsymbol{B}(f)$ and masked/unmasked $\boldsymbol{Y}(f,\tau)$, the local magnetic-field data are reconstructed. FDICA is applied to the two local electric-field data and two "raw" reference data as we do for the magnetic data and determine the electric-field signals (**PB5** in Figure 2, the same as **PB4**). Subsequently, we apply the median masking (**PD** in Figure 2) and reconstruct the electric-field signals.

Downloaded 01/04/21 to 130.54.110.22. Redistribution subject to SEG license or copyright; see Terms of Use at https://library.seg.org/page/policies/terms
DOI:10.1190/geo2018-0792.1

In the estimation of the MT response functions, the stacking of spectra described by Vozoff (1972) and the remote-reference processing described by Gamble et al. (1979a) are applied using raw reference data. Although the separated components are modeled by a specific distribution (i.e., a Laplace distribution), the reconstructed MT data from $\boldsymbol{B}(f)$ and $\boldsymbol{Y}(f,\tau)$ can be treated as well as the raw MT data with less noise because the data approach to Gaussian distributions by the central limit theorem (Hyvärinen et al., 2001). As a result, for error estimation, we use the method by Gamble et al. (1979b), which is a simple method based on error propagation. In this study, all of the estimated errors are derived with confidence levels of 95%.

It is important to note that the described method of signal-noise separation leads to cleaned raw spectra that can be used as input to any more advanced strategy for MT impedance estimation, such as bounded influence robust processing (Chave and Thomson, 2004). We use spectral stacking to illustrate the strength of the method in a simple example, but other methods would equally work.

APPLICATION TO MT DATA ACQUIRED AT KAKIOKA MAGNETIC OBSERVATORY

To confirm the effectiveness of FDICA-MT, we specifically examine the MT data acquired at the Kakioka Magnetic Observatory. High-quality MT responses are estimated by Fujii et al. (2015) on the basis of recent 11-year data at this observatory. Compared with the long-term responses, the response estimation from the short-term data enables a check of noise-reduction performance of FDICA-MT. We use 1 s sampling MT data between 1 March 2015 and 16 March 2015 (Figure 3a), and 1-minute sampling MT data between 1 February 2015 and 16 March 2015 (Figure 3b). The data set was obtained from the website of the Kakioka Magnetic Observatory (Kakioka Magnetic Observatory, 2015a, 2015b, 2015c, 2015d, 2015e, 2015f). To avoid the good S/N owing to large MT signal amplitudes, the duration was selected so that the average K index per 3.0 hours was below 2.0, indicating moderately quiet geomagnetic activity. In this study, magnetic-field data acquired at the Memambetsu Magnetic Observatory are used for reference data.

The MT responses by FDICA-MT are compared with those obtained using BIRRP version 5.3.2 (based on Chave and Thomson, 2004). We use one reference site (Memambetsu) for fair comparison, although BIRRP can treat any number of reference data. We apply STFT after detrending by the first-order difference filter. In the analysis for the 1 s sampling data, all spectra are the 7th–18th bins in each Fourier-transform length, and the same length is applied to the same frequency in BIRRP and FDICA-MT. When processing the 1-minute sampling data, we use the 10th–16th bins for FDICA-MT. But for BIRRP, we input spectra of the 5th–8th bins derived by halving the Fourier-transform length for FDICA-MT because more stable results are obtained. The other parameters in the BIRRP analysis are set based on default values that have yielded the best results (the parameters are provided as a data supplement). The analysis flow of the two codes, FDICA-MT and BIRRP, is summarized in Figure 4. In FDICA-MT, we divide the time-dependent

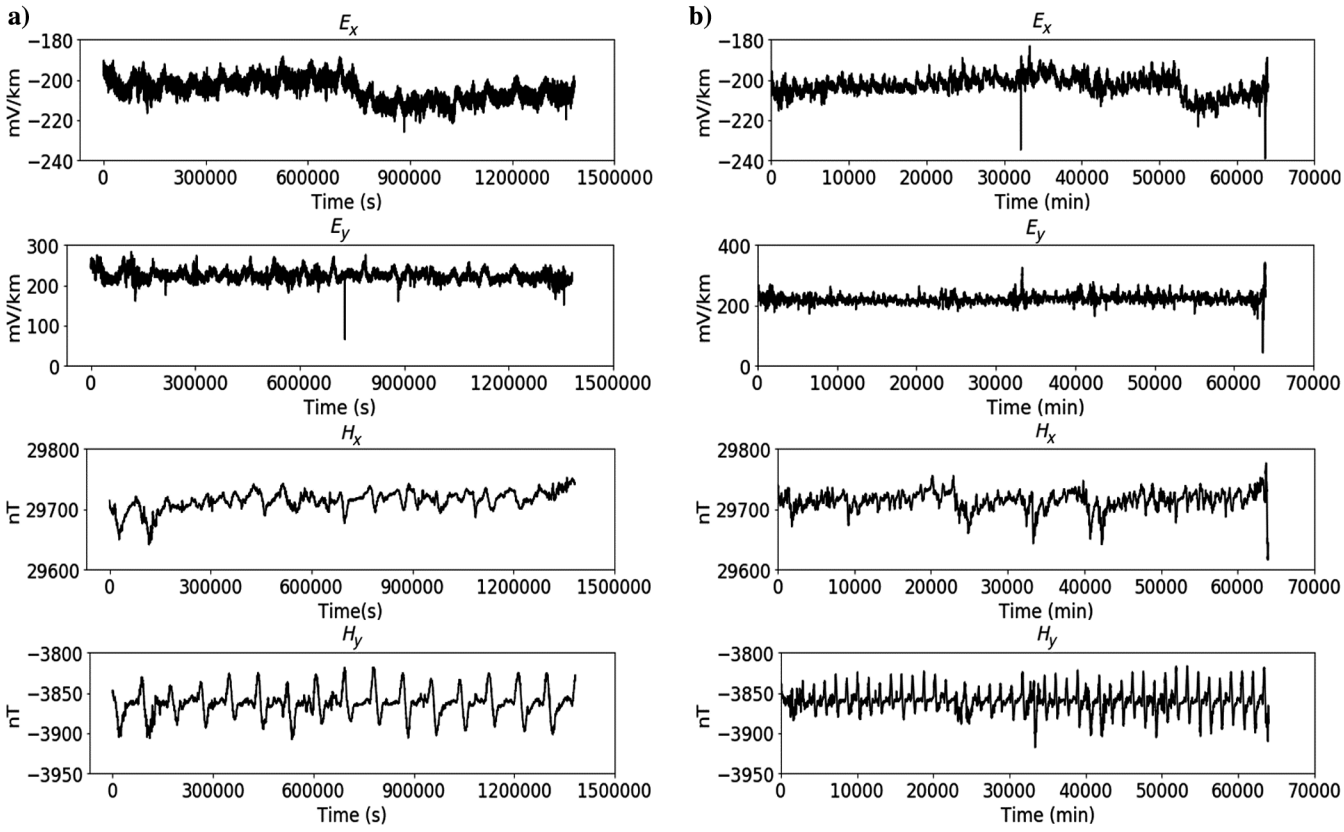

Figure 3. Raw MT data at Kakioka: (a) 1 s sampling MT data obtained during 1–16 March 2015 and (b) 1 minute sampling MT data obtained between 1 February 2015 and 16 March 2015.

Downloaded 01/04/21 to 130.54.110.22. Redistribution subject to SEG license or copyright; see Terms of Use at https://library.seg.org/page/policies/terms
DOI:10.1190/geo2018-0792.1

spectra to evaluate the signal-separation performance and we select the data sections to be analyzed based on "**PC**" (Figure 2). The entire spectra at periods longer than 43 s are analyzed, without dividing the data sections, because the effects of inherent noise seem small on the basis of m_{SN} and the total number of time windows is insufficient for division into many sections.

The MT response functions at Kakioka derived from the two methods are presented in Figure 5. Those at periods shorter than 341 s are derived from the 1 s sampling data, and those at longer periods are derived from the 1-minute sampling data. The responses by Fujii et al. (2015) derived from 11-year data processed by BIRRP are also indicated. The MT responses derived using FDICA-MT have smaller estimated errors and change more smoothly than BIRRP at the period band between 18 and 3072 s. Therefore, the FDICA-MT results also correspond to those by Fujii et al. (2015), which are based on the 11-year data, whereas the length of our data set is fewer than 1.5 months. It can therefore be inferred that FDICA-MT can maintain the accuracy of MT responses even if the number of analyzed spectra is substantially fewer than the conventional method, which is a great benefit for monitoring subsurface environments. However, discrepancies between the MT responses by FDICA-MT and those reported by Fujii et al. (2015) are observed at the period of 57–100 s. Moreover, it is noteworthy that at the periods shorter than 13 s and longer than 7680 s the apparent resistivity and phase curves by FDICA-MT show less-smooth features and large estimated errors. This can be explained as follows: At periods shorter than 13 s, (1) the low S/N at the local and reference sites interrupts the MT signal determination (i.e., the condition is far from equation 12) and (2) fewer spectra are available for stacking due to fewer selected data sections, and at periods longer than 7680 s, fewer spectra are obtainable owing to the long Fourier transform length.

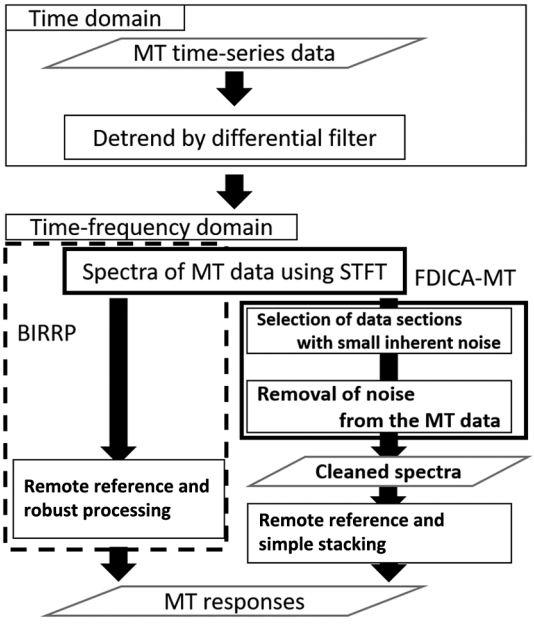

Figure 4. Flow of MT data analysis in this study. The process flow of FDICA-MT is explained in detail in Figure 2.

NOISE-REDUCTION PERFORMANCE

To quantitatively evaluate the noise-reduction performance of FDICA-MT, synthetic coherent noise was added to the raw MT data at Kakioka. All additional noise components in this section satisfy (1) each couple of the noise waveforms is independent, (2) all are coherent noise, and (3) formed by the combinations of rectangular waves and random noise. For a quantitative discussion related to noise-reduction performance, the apparent resistivity difference (ARD; %) is defined as

$$\mathrm{ARD} = \frac{|\rho_K - \rho_N|}{\rho_K} \times 100, \tag{15}$$

where ρ_K denotes the apparent resistivity derived from the raw MT data without synthetic noise by BIRRP or FDICA-MT (Figure 5) and ρ_N represents those derived from the MT data including the synthetic noise by BIRRP or FDICA-MT.

At first, two independent noise waveforms are prepared for the 1-minute sampling data at Kakioka (Figure 3b). An example of the EM waveforms, including the synthetic noise, is presented in Figure 6. The maximum noise amplitudes are adjusted to 200 mV/km in E_x, 1000 mV/km in E_y, and 6 nT in H_x and H_y in the case of Figure 6. The noise affects 63% of the time series in Figure 6. Here, we particularly examine the period range of 480–3072 s because the apparent resistivity curves obtained using BIRRP and FDICA-MT (Figure 5) show smooth features over this range with small estimated errors and correspond to the curves derived from the long-term data (Fujii et al., 2015). The study quantitatively evaluates the noise-reduction performance by BIRRP and FDICA-MT. However, BIRRP degradation can be expected because it theoretically breaks down at 50% noise contamination, as shown in Figure 5a.

As a result, we successfully obtain the apparent resistivity curves using FDICA-MT, although the MT data include large synthetic noise. Figure 7 is an example of MT responses derived from the noisy data (Figure 6) using BIRRP and FDICA-MT. As shown in Figure 7, the average ARD (equation 15) of ρ_{xy} and ρ_{yx} obtained by BIRRP is 105% and 5%, respectively, whereas the average ARD obtained using FDICA-MT is only 9% and 7%. The phases derived from the noisy data indicate similar features to the apparent resistivity, and the FDICA-MT results are similar to the case of no synthetic noise. We therefore only focus on apparent resistivity in the following section for the sake of simplicity.

We vary the noise amplitude and contamination time span to evaluate the relation between ARD and the noise level. Two independent time series of noise are assumed here, with amplitudes of 50 or 200 mV/km in E_x, 250 or 1000 mV/km in E_y, and 6 nT in H_x and H_y. The noise contamination time span is 40%, 56%, 63%, 81%, or 94% of the time series. In all cases and frequencies, $m_{\mathrm{SN}}(x, f)$ and $m_{\mathrm{SN}}(y, f)$ are greater than one. The relationships between the noise contamination time span and the average ARD by BIRRP and FDICA-MT are summarized in Figure 8 over the period range of 480–3072 s. In FDICA-MT, the average ARD of the contaminated data is less than 20% even at the longest noise contamination time span.

For testing noisier cases, four independent synthetic noise components are added to the 1 minute sampling raw data, whereas previous cases used only two. In general, the conventional FDICA for MT can accommodate a case in which noise components are limited

Downloaded 01/04/21 to 130.54.110.22. Redistribution subject to SEG license or copyright; see Terms of Use at https://library.seg.org/page/policies/terms
DOI:10.1190/geo2018-0792.1

to two when two MT signal components exist. This test elucidates the robustness of FDICA-MT in the case of many origins of noise (i.e., the number of all sources is greater than four). The four time series of noise have maximum amplitudes of 50 or 200 mV/km in E_x, 250 or 1000 mV/km in E_y, and 4 or 20 nT in H_x and H_y. When the noise with 20 nT as the maximum amplitude is added to the magnetic field, m_{SN} becomes less than one. If noise of 4 nT maximum amplitude is included, m_{SN} also drops to less than one at short periods (approximately 1000 s). We applied FDICA-MT to these noisy data and derived the MT responses and ARD. The resultant ARD and estimated errors of the apparent resistivity are presented in Figure 9, similarly to Figure 8. In FDICA-MT, the average ARD is also less than 20% but it remains low up to a noise contamination time span below 63%. The estimated errors of FDICA-MT results (Figure 9d) are again smaller than those obtained by BIRRP (Figure 9c).

Finally, we add two independent time series of synthetic noise to the 1 s sampling MT data (Figure 3a), where originally large noise was mixed. The two coherent noise components have amplitudes of 200 mV/km in E_x and E_y, and 4 nT in H_x and H_y. They are added to the raw MT data with varied noise contamination time span (i.e., 40%, 56%, 63%, 81%, or 94%). Using these data sets, we evaluate the noise-reduction performance of FDICA-MT on the basis of average ARD over the range of 57–170 s. In these tests, under a high-level noise environment, the m_{SN} are all greater than one. The results are presented in Figure 10. The average ARD remains at less than 20% if the noise contamination time span is less than 81%.

DISCUSSION

Discussion on the analysis of raw MT data at Kakioka

Here, we discuss the cause of discrepancies between the responses by FDICA-MT and those reported by Fujii et al. (2015), effects of data section length, and the origin of noise included in the MT data at Kakioka.

At the periods of 57–100 s, the MT responses by FDICA-MT (Figure 5) have small estimated errors, but they indicate a difference from the responses by Fujii et al. (2015). This is because the response functions at this period band are derived from relatively short-term data (within 16 days) and are possibly affected by instability of the source field. The source field's effect on the MT response has been reported in many studies (Egbert et al., 2000; Brändlein et al., 2012; Romano et al., 2014; Murphy and Egbert, 2018). Romano et al. (2014) conclude that MT responses at the period bands especially at approximately 20–100 s are unstable when the Ap index, the magnitude of geomagnetic activity, is smaller than

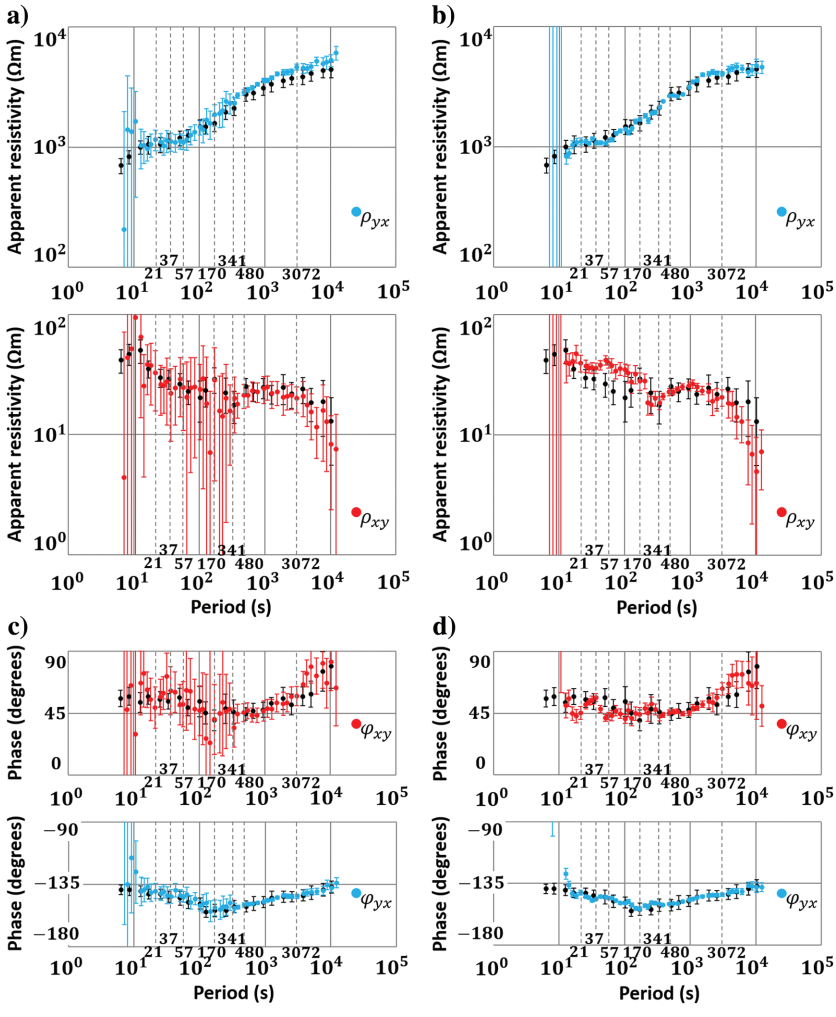

Figure 5. MT response curves. Apparent resistivity derived using (a) BIRRP and (b) FDICA-MT. Phases by (c) BIRRP and (d) FDICA-MT. The responses at periods shorter than 341 s are derived from the 1 s sampling data, and those at longer periods are derived from the 1 minute sampling data. The black curves depicted in (a-d) are the apparent resistivity or phase derived from the MT data obtained during 2000–2011 (Fujii et al., 2015). All estimated errors are within a confidence level of 95%.

Downloaded 01/04/21 to 130.54.110.22. Redistribution subject to SEG license or copyright; see Terms of Use at https://library.seg.org/page/policies/terms
DOI:10.1190/geo2018-0792.1

10. They also report a negative correlation between the apparent resistivity and the Ap index, such that a smaller Ap index is associated with a larger apparent resistivity. In our study, the apparent resistivity obtained by FDICA-MT is based on MT data under the average K index per 3.0 hours at less than 2.0, corresponding to an Ap index of 6. The apparent resistivity reported by Fujii et al. (2015) is based on the 11-year geomagnetic fluctuations and is not affected by the source field, although our results are affected. These situations, such as the period band, magnitude of geomagnetic activity, and increase in apparent resistivity based on the short-term MT data (within 16 days), are similar to the result reported by Romano et al. (2014). We derived the MT responses during 16–20 March in 2015 when the average K index was moderately high (3.45) and with Ap index of 18 (provided as a data supplement). They correspond to the response of the 11-year data, supporting the above implication on the cause of differences between the two MT responses.

At the short period band between 7 and 37 s, we selected the data sections following **PC** (Figure 2). The appropriate length of the divided sections must be discussed because each section length might affect the obtained MT responses. For example, focusing on the period of 21 s, we vary the total number of time windows in each section from 42 to 5400. Note that the Fourier-transform length is fixed at 256 s and derives the responses. The results show that a data section length between 168 and 1800 provides similar MT responses. At other periods (21–37 s), the short-side limitation of each section for the stable evaluation of the MT responses is 168 time windows based on the smoothness/consistency through the frequencies. Although the most suitable length of data sections should be found varying the Fourier transform length, our trial-and-error approach with each section having more than 100 time windows is considered to be acceptable.

To confirm whether the FDICA-MT properly rejects the cultural noise using "**PB1-5**" and "**PD**" (Figure 2), we reconstruct the time series of noise components. This study specifically examines the periods with small estimated errors in FDICA-MT: 57–170 s in the 1 s sampling data and 480–3072 s in the 1 minute sampling data. Figure 11a shows the time series of noise extracted from the 1 s data, which is obtained by inverse Fourier transform. Figure 11b is also the time series of noise, for which the original sampling is 1 minute. In Figure 11a, high-amplitude noise is clearly observable in the daytime, but during the night (00:00–04:00 am) the noise has smaller amplitudes. In Figure 11b, the noise is apparent during the daytime and nighttime, but the amplitude is smaller in the latter. On the basis of the environment near the observatory, the cultural noise in the MT data at Kakioka can be considered to come from a distant urban area (e.g., Tokyo), and, as a result, the noise seems to correlate with human activity. However, at the period band of 480–3072 s, the BIRRP and FDICA-MT yield small estimated errors of the MT response functions and are similar to the high-quality responses based on the long-term data by Fujii et al. (2015) (Figure 5). This suggests that the noise contamination of the 1 minute sampling data at Kakioka is not severe. We can also better understand why the FDICA-MT succeeded in processing the 1 s data. As shown in Figure 11a, the noise contaminates most parts of the data, whereas the FDICA-MT is robust to such a continuous noise as shown in Figures 8–10. Therefore, MT response functions can be derived with high accuracy using FDICA-MT.

Magnetic data records at Kakioka have been well maintained over many years and may be believed to be under noise-free conditions. The cultural noise is removed from the data with 1 minute and hourly sampling rates by the historical effort of the magnetic

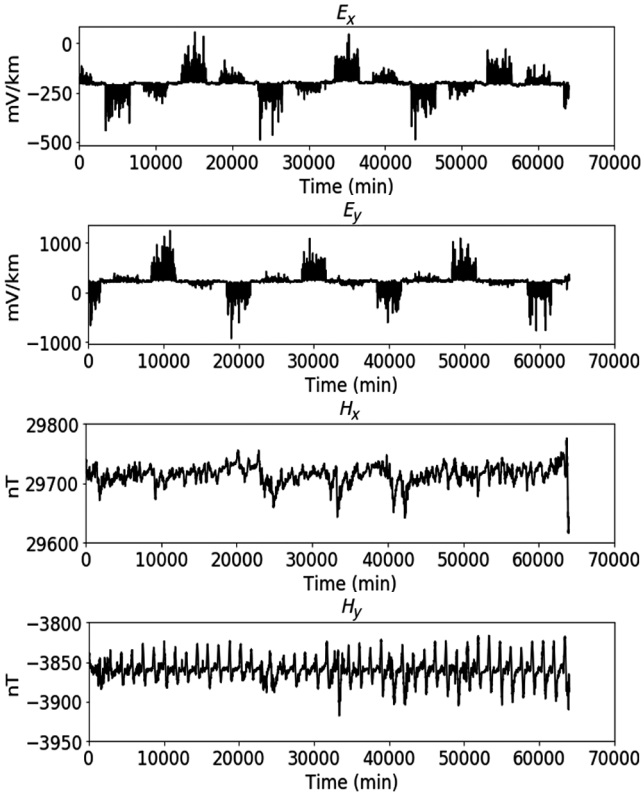

Figure 6. The 1 minute sampling MT data with synthetic coherent noise. The original raw time series are shown in Figure 3b. The noise has a maximum amplitude of 200 mV/km in E_x, 1000 mV/km in E_y, and 6 nT in H_x and H_y. The noise contamination time span is 63% of the time series.

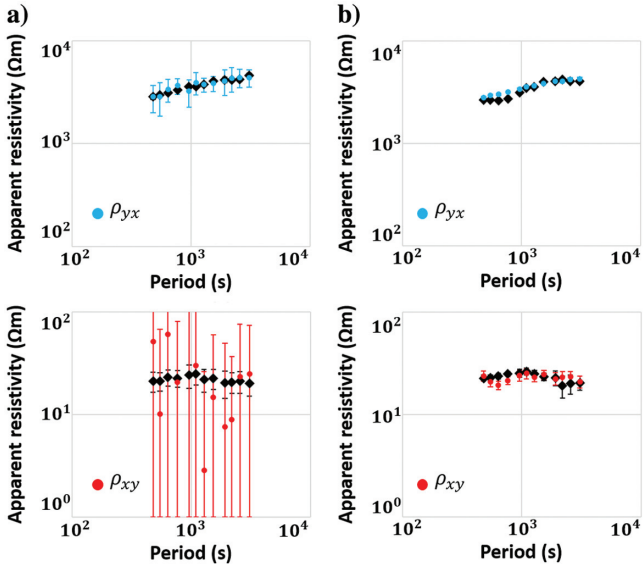

Figure 7. Apparent resistivity curves derived from the MT data with synthetic noise: (a) BIRRP and (b) FDICA-MT. The black diamonds represent the responses derived from raw MT data.

observatory (Kakioka Magnetic Observatory, 2019). However, MT data with a 1 s sampling rate possibly contain cultural noise (Kakioka Magnetic Observatory, 2019). It is difficult to derive MT responses with small estimated errors from the short-time data with a 1 s sampling rate, as shown in the BIRRP results. This indicates that the data with a 1 s sampling rate include some cultural noise, as shown in Figure 11a. The data set with a 1 s sampling rate can be considered suitable for validating our FDICA-MT.

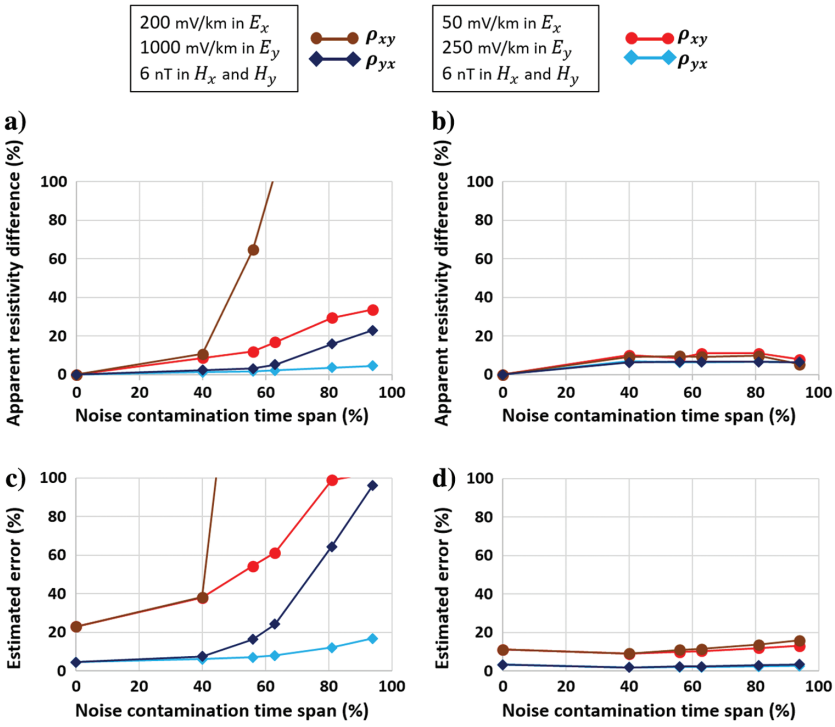

Figure 8. (a) Correlation between the noise condition and the average ARD (equation 15) by BIRRP in the range of 480–3072 s. The vertical axis shows the average ARD between the raw MT data and MT data with two synthetic noise components. The horizontal axis shows the noise contamination time span. The red and light-blue lines show the results obtained under the condition in which two noise components have maximum amplitudes of 50 mV/km in E_x, 250 mV/km in E_y, and 6 nT in H_x and H_y. The brown and dark-blue lines show the results obtained under the conditions in which two noise components have maximum amplitudes of 200 mV/km in E_x, 1000 mV/km in E_y, and 6 nT in H_x and H_y. The circles represent the average ARD of ρ_{xy}. The diamonds are the average ARD of ρ_{yx}. (b) Correlation between the noise condition and the average ARD derived using FDICA-MT. (c) Average estimated errors of apparent resistivity derived using BIRRP. (d) Average estimated errors obtained using FDICA-MT.

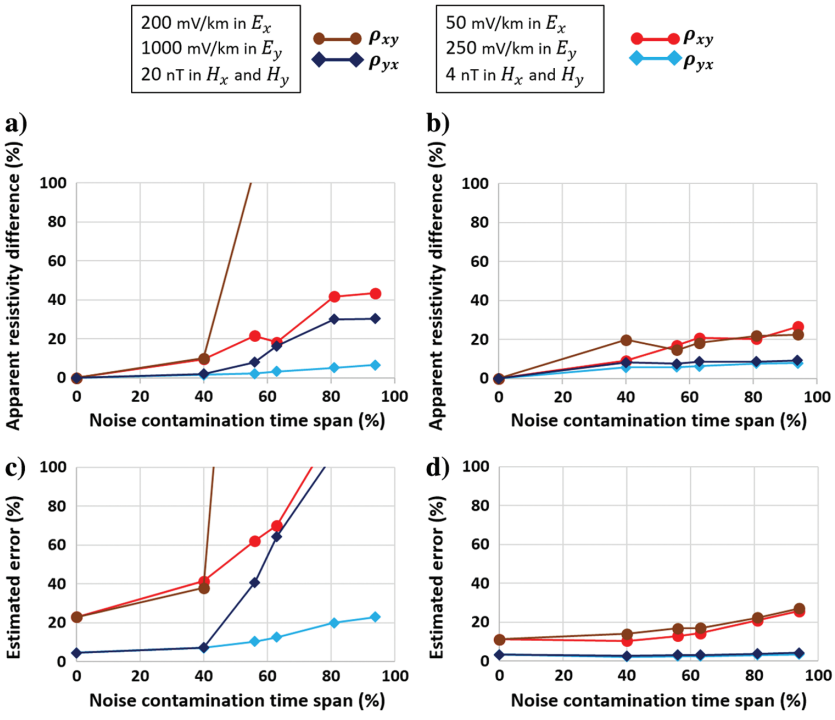

Figure 9. (a) Correlation between the noise condition and the average ARD (equation 15) by BIRRP in the range of 480–3072 s. The vertical axis shows the average ARD between the raw MT data and the MT data with four synthetic noise components. The horizontal axis shows the noise contamination time span. The red and light-blue lines show the results obtained under the condition of four noise components with maximum amplitudes of 50 mV/km in E_x, 250 mV/km in E_y, and 4 nT in H_x and H_y. The brown and dark-blue lines obtained under the conditions with two noise components with amplitudes of 200 mV/km in E_x, 1000 mV/km in E_y, and 20 nT in H_x and H_y. The circles represent the average ARD of ρ_{xy}. The diamonds are the average ARD of ρ_{yx}. (b) Correlation between the noise condition and the average ARD derived using FDICA-MT. (c) Average estimated errors of apparent resistivity derived using BIRRP. (d) Average estimated errors using FDICA-MT.

Downloaded 01/04/21 to 130.54.110.22. Redistribution subject to SEG license or copyright; see Terms of Use at https://library.seg.org/page/policies/terms
DOI:10.1190/geo2018-0792.1

Downloaded 01/04/21 to 130.54.110.22. Redistribution subject to SEG license or copyright; see Terms of Use at https://library.seg.org/page/policies/terms
DOI:10.1190/geo2018-0792.1

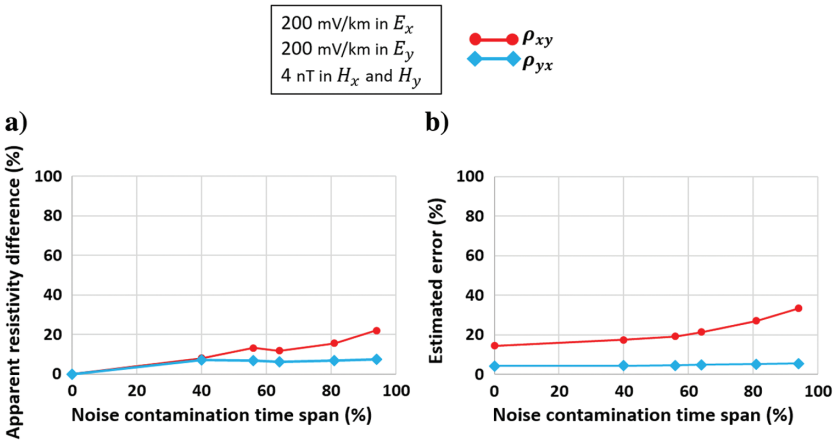

Figure 10. (a) The vertical axis shows the average ARD (equation 15) between the raw MT data and the MT data with two synthetic noise components of 57–170 s. The horizontal axis shows the noise contamination time span. The two noise components have amplitudes of 200 mV/km in E_x and E_y and 4 nT in H_x and H_y. The red circles represent the average ARD of ρ_{xy}. The light-blue diamonds are the average ARD of ρ_{yx}. (b) Average estimated errors of apparent resistivity derived by FDICA-MT from the MT data with synthetic noise.

Discussion on the noise-reduction performance of FDICA-MT

The results of the application to the noisy data, which combine the two synthetic noise components and 1 minute raw data, show that the FDICA-MT performance is independent of the noise amplitude and noise contamination time span. Although the accuracy of the derived MT responses depends on the noise levels, the estimated errors are comparable to the observed temporal changes of responses, such as around volcanic regions as potential geothermal energy sources (e.g., 20% of the apparent resistivity, Aizawa et al., 2011). Our method can be sufficiently useful to monitor subsurface phenomena such as volcanic eruptions. The noisy MT data here include (1) two dominant MT signals, (2) two large synthetic noise components, and (3) other small noise originally included in the raw data (Figure 11b). FDICA-MT can be expected to process MT data contaminated by high-level noise if the number of large noise components is limited to two and if the S/N of the local magnetic field (or remote site) is sufficiently high.

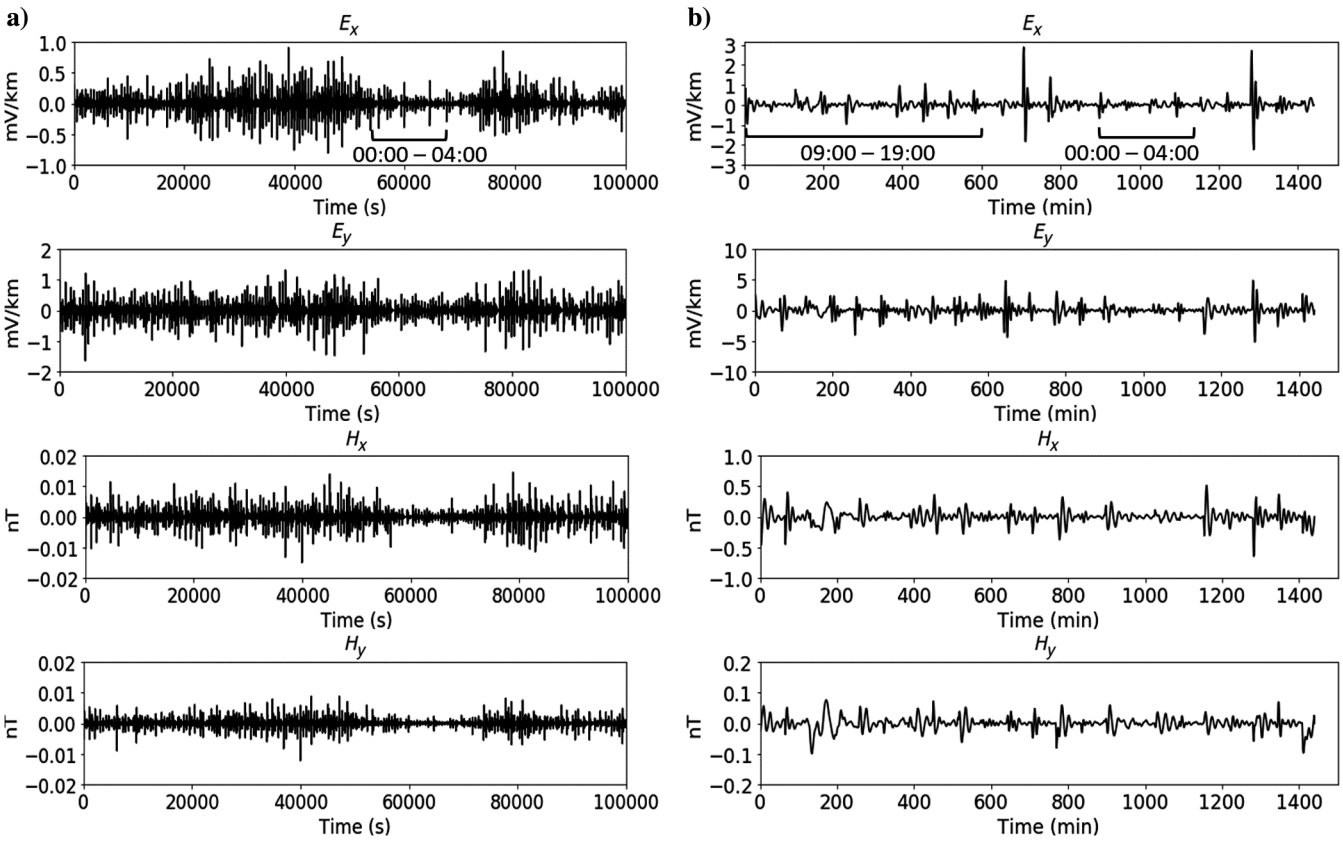

Figure 11. (a) Noise extracted by FDICA-MT from the raw MT data on March 1 (1 s sampling) at Kakioka included in the range of 57–170 s. (b) Noise extracted by FDICA-MT from the raw MT data obtained on March 1 (1 minute sampling) at Kakioka in the range of 480–3072 s.

Downloaded 01/04/21 to 130.54.110.22. Redistribution subject to SEG license or copyright; see Terms of Use at https://library.seg.org/page/policies/terms
DOI:10.1190/geo2018-0792.1

Under the condition that the four synthetic noise components are added to the 1 minute sampling raw data, the noise-reduction performance of FDICA-MT can retain a sufficiently high level if the noise contamination time span is less than 63% (Figure 9b and 9d). In cases of low S/N of magnetic-field data, we apply FDICA twice, and the effect of remaining noise can be considered large. Additionally, in the case of a high S/N, there are more than four components, and this can be considered to cause the large amount of remaining noise.

Based on the results of FDICA-MT noise-reduction performance in the 1 s sampling data (Figure 10), as with the four synthetic noise components in the 1 minute data (Figure 9b and 9d), the noise-reduction performance of FDICA-MT is satisfactory if the noise contamination time span is less than 81%. From noise components extracted from the raw data (Figure 11a), we ascertain that the cultural noise is included in the 1 s sampling raw data. Therefore, the reason for the degradation of the noise-reduction performance under the noise contamination time span greater than 81% is the same as the case of adding four noise components. Consequently, four or more large noise components strongly interrupt the estimation of MT responses with high accuracy, although we infer that two large noise components can be removed properly using FDICA-MT.

CONCLUSION

This study proposes an algorithm of FDICA for application to MT data (FDICA-MT), within which four major modifications are adopted. First, a method to estimate the minimum S/N of local magnetic-field data is developed. Second, a criterion of separated components on the basis of the S/N of magnetic field data is set. Third, we develop a method to select data sections with small inherent noise for good signal-separation performance. Finally, a method is developed to extract MT signals in separated components regarded as noise.

FDICA-MT is applied to the raw MT data obtained at Kakioka. A comparison with the responses derived using a conventional method, BIRRP, shows that the response curves obtained using FDICA-MT are smoother and their errors are smaller. We conclude that the FDICA-MT is a powerful estimator of MT responses even if most of the time-series data are contaminated by cultural noise. It also indicates that MT response functions can be derived even from short-term data because the long-term data for stacking (i.e., reducing noise) are not required.

Finally, we test the noise-reduction performance by applying FDICA-MT to noisy MT data. Although the analyzed data are limited, our FDICA-MT algorithm is considered effective for MT data analysis under the following conditions. If the S/N of the magnetic field at the local site is satisfactory and if only two large noise components are mixed, then FDICA-MT yields highly accurate MT responses from noisy data. If the S/N of the magnetic field is not sufficiently high or if there are several large noise components, FDICA-MT should be applied under the condition that the reference data have a high S/N. Even if the conditions cannot be achieved, the obtained MT responses using FDICA-MT yield higher quality results than those produced using conventional methods.

The FDICA-MT provides the opportunity to obtain MT responses from shorter data so it can be applied to monitoring volcanic activity, geothermal fields, and hydrocarbon reservoirs even in high-noise environments. This important advantage over conventional processing is expected to be beneficial for the estimation of MT responses in highly populated areas for disaster prevention (e.g., around active faults in urban areas) and relevant environmental studies.

ACKNOWLEDGMENTS

The authors appreciate A. Chave of the Woods Hole Oceanographic Institution for the use of his code BIRRP. We appreciate the use of data from the Kakioka Magnetic Observatory, Japan. Further, we thank K. Koike and I. Fujii for the helpful comments. This study is supported by the Ministry of Education, Culture, Sports, Science and Technology of Japan, in grant-in-aid for Scientific Research (JSPS KAKENHI grant nos. JP26289347, JP18J20941, and JP18H03894). Finally, the authors thank X. Garcia and the anonymous reviewers for their constructive criticism.

DATA AND MATERIALS AVAILABILITY

Data associated with this research are available and can be obtained by contacting the corresponding author.

APPENDIX A

A CALCULATION METHOD FOR S/N OF LOCAL MAGNETIC-FIELD DATA

Local magnetic-field data $\boldsymbol{H}_x(f)$ and reference magnetic-field data $\boldsymbol{R}_x(f)$ at a frequency can be represented as

$$\boldsymbol{H}_x(f) = \boldsymbol{S}(f) + \boldsymbol{N}_L(f), \tag{A-1}$$

$$\boldsymbol{R}_x(f) = \boldsymbol{S}(f) + \boldsymbol{N}_R(f), \tag{A-2}$$

where $\boldsymbol{S}(f) = \{S(f,1), \ldots, S(f,T)\}^{\mathrm{tr}}$ is the MT signal, and $\boldsymbol{N}_L(f) = \{N_L(f,1), \ldots, N_L(f,T)\}^{\mathrm{tr}}$ and $\boldsymbol{N}_R(f) = \{N_R(f,1), \ldots, N_R(f,T)\}^{\mathrm{tr}}$ are noise at the local and reference sites, respectively. Under the assumption that the MT signal $\boldsymbol{S}$ and noise ($\boldsymbol{N}_R$ and $\boldsymbol{N}_L$) are independent (i.e., $\left\langle \boldsymbol{S}, \boldsymbol{N}_L^* \right\rangle = \left\langle \boldsymbol{S}, \boldsymbol{N}_R^* \right\rangle = \left\langle \boldsymbol{N}_L, \boldsymbol{N}_R^* \right\rangle = 0$) and by substituting equations A-1 and A-2 for the first and second terms on the right side of equation 9, we obtain

$$\frac{\langle (\boldsymbol{S}+\boldsymbol{N}_R)^*, (\boldsymbol{S}+\boldsymbol{N}_L) \rangle}{\langle (\boldsymbol{S}+\boldsymbol{N}_R)^*, (\boldsymbol{S}+\boldsymbol{N}_R) \rangle} (\boldsymbol{S}+\boldsymbol{N}_R) = \frac{|\boldsymbol{S}|^2}{|\boldsymbol{S}|^2 + |\boldsymbol{N}_R|^2} (\boldsymbol{S}+\boldsymbol{N}_R), \tag{A-3}$$

$$\begin{aligned} &(\boldsymbol{S}+\boldsymbol{N}_L) - \frac{\langle (\boldsymbol{S}+\boldsymbol{N}_R)^*, (\boldsymbol{S}+\boldsymbol{N}_L) \rangle}{\langle (\boldsymbol{S}+\boldsymbol{N}_R)^*, (\boldsymbol{S}+\boldsymbol{N}_R) \rangle} (\boldsymbol{S}+\boldsymbol{N}_R) \\ &= (\boldsymbol{S}+\boldsymbol{N}_L) - \frac{|\boldsymbol{S}|^2}{|\boldsymbol{S}|^2 + |\boldsymbol{N}_R|^2} (\boldsymbol{S}+\boldsymbol{N}_R) \\ &= \boldsymbol{N}_L + \frac{|\boldsymbol{N}_R|^2 \boldsymbol{S} - |\boldsymbol{S}|^2 \boldsymbol{N}_R}{|\boldsymbol{S}|^2 + |\boldsymbol{N}_R|^2}. \end{aligned} \tag{A-4}$$

Dividing the squared Euclidean of equation A-3 by equation A-4 gives

Downloaded 01/04/21 to 130.54.110.22. Redistribution subject to SEG license or copyright; see Terms of Use at https://library.seg.org/page/policies/terms
DOI:10.1190/geo2018-0792.1

$$\frac{|\frac{\boldsymbol{R}_x^*\boldsymbol{H}_x}{\boldsymbol{R}_x^*\boldsymbol{R}_x}\boldsymbol{R}_x|^2}{|\boldsymbol{H}_x-\frac{\boldsymbol{R}_x^*\boldsymbol{H}_x}{\boldsymbol{R}_x^*\boldsymbol{R}_x}\boldsymbol{R}_x|^2}=\frac{|\frac{|\boldsymbol{S}|^2}{|\boldsymbol{S}|^2+|\boldsymbol{N_R}|^2}(\boldsymbol{S}+\boldsymbol{N_R})|^2}{|\boldsymbol{N}_L+\frac{|\boldsymbol{N_R}|^2\boldsymbol{S}-|\boldsymbol{S}|^2\boldsymbol{N_R}}{|\boldsymbol{S}|^2+|\boldsymbol{N_R}|^2}.|^2}$$
$$=\frac{\frac{|\boldsymbol{S}|^4(|\boldsymbol{S}|^2+|\boldsymbol{N_R}|^2)}{(|\boldsymbol{S}|^2+|\boldsymbol{N_R}|^2)^2}}{|\boldsymbol{N}_L|^2+\frac{|\boldsymbol{S}|^2|\boldsymbol{N_R}|^2(|\boldsymbol{S}|^2+|\boldsymbol{N_R}|^2)}{(|\boldsymbol{S}|^2+|\boldsymbol{N_R}|^2)^2}}$$
$$=\frac{\frac{|\boldsymbol{S}|^4}{(|\boldsymbol{S}|^2+|\boldsymbol{N_R}|^2)}}{|\boldsymbol{N}_L|^2+\frac{|\boldsymbol{S}|^2|\boldsymbol{N_R}|^2}{(|\boldsymbol{S}|^2+|\boldsymbol{N_R}|^2)}}$$
$$=\frac{|\boldsymbol{S}|^4}{|\boldsymbol{S}|^2|\boldsymbol{N}_L|^2+|\boldsymbol{S}|^2|\boldsymbol{N_R}|^2+|\boldsymbol{N_R}|^2|\boldsymbol{N}_L|^2}$$
$$\le\frac{|\boldsymbol{S}|^2}{|\boldsymbol{N}_L|^2}. \tag{A-5}$$

The equality can be established only when there is no noise in the reference data ($|\boldsymbol{N_R}|=0$). The left side of the first line in equation A-5, which is equal to the squared $m_{\mathrm{SN}}(x,f)$ in equation 10, is the minimum value of the right side of the fifth line, which is equal to the squared S/N of the local magnetic-field data. The ratio will be downward biased by noise in the reference data. We can therefore conclude that m_{SN} is always smaller than the true S/N.

APPENDIX B

THE REASON FOR SETTING STEPPED THRESHOLDS

In this study, we select noise components based on a continuous threshold if the number of MT signals in the four separated components is limited to one. However, a stepped threshold is required when there are two (general case) or more MT signals. To prevent the extraction of the noise component as an MT signal, we briefly focus on the relationship between m_{SN} (equation 10) and the inverse of separation matrix $\boldsymbol{B}(f)$ (equation 5) in the x-direction. Let us consider that only one MT signal exists, although such a case is not realistic. We determine only one separated component as the MT signal, and the relationship can be established using the $\boldsymbol{B}(f)$:

$$\frac{1}{m_{\mathrm{SN}}(x,f)}\ge\frac{\sum|B(f)_{\text{noise in }H_x}|}{\sum|B(f)_{\text{signal in }H_x}|}\ge\frac{|B(f)_{\text{noise in }H_x}|}{\sum|B(f)_{\text{signal in }H_x}|}$$
$$=\frac{|B(f)_{\text{noise in }H_x}|}{\max_k|B(f)_{3k}|}, \tag{B-1}$$

where $B(f)_{\text{noise in }H_x}$ and $B(f)_{\text{signal in }H_x}$ are elements of $\boldsymbol{B}(f)$ and denote the contribution of the noise and MT signal components to H_x, respectively. The expression $\sum|B(f)_{\text{noise in }H_x}|/\sum|B(f)_{\text{signal in }H_x}|$ in equation B-1, which is the summation of all $|B(f)_{\text{noise in }H_x}|$ over the summation of all $|B(f)_{\text{signal in }H_x}|$, denotes the reciprocal S/N of H_x calculated from the FDICA result. If equation B-1 is established, we can then determine the noise components on the basis of a continuous threshold that $|B(f)_{\text{noise in }H_x}|$ is smaller than $\max_k|B(f)_{3k}|/m_{\mathrm{SN}}(x,f)$. However, when two (general case) or more MT signals exist, we obtain the relationship as

$$\frac{|B(f)_{\text{noise in }H_x}|}{\max_k|B(f)_{3k}|}>\frac{|B(f)_{\text{noise in }H_x}|}{\sum|B(f)_{\text{signal in }H_x}|}\le\frac{1}{m_{\mathrm{SN}}(x,f)}. \tag{B-2}$$

Based on equation B-2, in such a general case, we cannot ensure that the contribution of a noise component holds $|B(f)_{\text{noise in }H_x}|\le\max_k|B(f)_{3k}|/m_{\mathrm{SN}}(x,f)$, which is obtained from equation B-1. The possibility of holding $|B(f)_{\text{noise in }H_x}|>\max_k|B(f)_{3k}|/m_{\mathrm{SN}}(x,f)$ should therefore be considered. As a result, if we set a continuous threshold for the signal determination of FDICA, the noise components are possibly extracted as MT signals when two or more signal components exist. We should therefore prepare the margin and set the threshold as stepped rather than continuous to prevent this mistake. Moreover, the largest contributions to the magnetic-field data do not likely correspond exactly to each magnetic-field data (e.g., $Y_3(f,\tau)$ with a maximum value in the contribution to $H_x(f,\tau)$ and $H_y(f,\tau)$). Even in such a case, by selecting the separated components with a large contribution to the magnetic field data following equation 11, we can identify which separated components correspond to the MT signals.

REFERENCES

Aizawa, K., W. Kanda, Y. Ogawa, M. Iguchi, A. Yokoo, H. Yakiwara, and T. Sugano, 2011, Temporal changes in electrical resistivity at Sakurajima volcano from continuous magnetotelluric observations: Journal of Volcanology and Geothermal Research, **199**, 165–175, doi: 10.1016/j.jvolgeores.2010.11.003.

Amari, S. I., A. Cichocki, and H. H. Yang, 1996, A new learning algorithm for blind signal separation: Advances in Neural Information Processing Systems, 757–763.

Brändlein, D., H. Lühr, and O. Ritter, 2012, Direct penetration of the interplanetary electric field to low geomagnetic latitudes and its effect on magnetotelluric sounding: Journal of Geophysical Research, Space Physics, **117**, A11314, doi: 10.1029/2012JA018008.

Chave, A. D., 2017, Estimation of the magnetotelluric response function: The path from robust estimation to a stable maximum likelihood estimator: Surveys in Geophysics, **38**, 837–867, doi: 10.1007/s10712-017-9422-6.

Chave, A. D., and D. J. Thomson, 2004, Bounded influence magnetotelluric response function estimation: Geophysical Journal International, **157**, 988–1006, doi: 10.1111/j.1365-246X.2004.02203.x.

Chave, A. D., D. J. Thomson, and M. E. Ander, 1987, On the robust estimation of power spectra, coherences, and transfer functions: Journal of Geophysical Research, Solid Earth, **92**, 633–648, doi: 10.1029/JB092iB01p00633.

Cui, J. L., M. Deng, J. E. Jing, and E. C. Wang, 2013, Using independent component analysis to process magnetotelluric data, *in* X. Tang, W. Zhong, D. Zhuang, C. Li, and Y. Liu, eds., Applied Mechanics and Materials: Trans Tech Publications, **295**, 2795–2798, doi: 10.4028/www.scientific.net/AMM.295-298.2795.

Egbert, G. D., 1997, Robust multiple-station magnetotelluric data processing: Geophysical Journal International, **130**, 475–496, doi: 10.1111/j.1365-246X.1997.tb05663.x.

Egbert, G. D., 2002, Processing and interpretation of electromagnetic induction array data: Surveys in Geophysics, **23**, 207–249, doi: 10.1023/A:1015012821040.

Egbert, G. D., and J. R. Booker, 1986, Robust estimation of geomagnetic transfer functions: Geophysical Journal International, **87**, 173–194, doi: 10.1111/j.1365-246X.1986.tb04552.x.

Egbert, G. D., M. Eisel, O. S. Boyd, and H. F. Morrison, 2000, DC trains and Pc3s: Source effects in mid-latitude geomagnetic transfer functions: Geophysical Research Letters, **27**, 25–28, doi: 10.1029/1999GL008369.

Fujii, I., T. Ookawa, S. Nagamachi, and T. Owada, 2015, The characteristics of geoelectric fields at Kakioka, Kanoya, and Memambetsu inferred from voltage measurements during 2000 to 2011: Earth, Planets and Space, **67**, 62, doi: 10.1186/s40623-015-0241-z.

Gamble, T. D., W. M. Goubau, and J. Clarke, 1979a, Magnetotellurics with a remote magnetic reference: Geophysics, **44**, 53–68, doi: 10.1190/1.1440923.

Gamble, T. D., W. M. Goubau, and J. Clarke, 1979b, Error analysis for remote reference magnetotellurics: Geophysics, **44**, 959–968, doi: 10.1190/1.1440988.

Downloaded 01/04/21 to 130.54.110.22. Redistribution subject to SEG license or copyright; see Terms of Use at https://library.seg.org/page/policies/terms
DOI:10.1190/geo2018-0792.1

He, Z., Z. Hu, Y. Gao, L. He, C. Meng, and L. Yang, 2015, Field test of monitoring gas reservoir development using time-lapse continuous electromagnetic profile method: Geophysics, **80**, no. 2, WA127–WA134, doi: 10.1190/geo2014-0195.1.

Hiroe, A., 2009, Frequency domain independent component analysis free from the permutation problem: IEICE Transactions on Fundamentals of Electronics, Communications and Computer Sciences (Japanese Edition), **92-A**, 286–293.

Hyvärinen, A., J. Karhunen, and E. Oja, 2001, Independent component analysis: John Wiley & Sons.

Hyvärinen, A., and E. Oja, 2000, Independent component analysis: Algorithms and applications: Neural networks, **13**, 411–430, doi: 10.1016/S0893-6080(00)00026-5.

Ikelle, L., 2007, Coding and decoding: Seismic data modeling, acquisition and processing: 77th Annual International Meeting, SEG, Expanded Abstracts, 66–70, doi: 10.1190/1.2792383.

Imamura, N., T. Goto, T. Kasaya, and H. Machiyama, 2017, Robust data processing of noisy marine controlled-source electromagnetic data using independent component analysis: Exploration Geophysics, **49**, 21–29, doi: 10.1071/EG17139.

Junge, A., 1996, Characterization of and correction for cultural noise: Surveys in Geophysics, **17**, 361–391, doi: 10.1007/BF01901639.

Kakioka Magnetic Observatory, 2015a, Kakioka geoelectric field 1-minute digital data in IAGA-2002 format, data set accessed 9 December 2016 at http://www.kakioka-jma.go.jp/obsdata/metadata/ja/products/2508/.

Kakioka Magnetic Observatory, 2015b, Kakioka geoelectric field 1-second digital data in IAGA-2002 format, data set accessed 17 June 2017 at http://www.kakioka-jma.go.jp/obsdata/metadata/ja/products/2509/.

Kakioka Magnetic Observatory, 2015c, Kakioka geomagnetic field 1-minute digital data in IAGA-2002 format, data set accessed 9 December 2016 at http://www.kakioka-jma.go.jp/obsdata/metadata/ja/products/2485/.

Kakioka Magnetic Observatory, 2015d, Kakioka geomagnetic field 1-second digital data in IAGA-2002 format, data set accessed 17 June 2017 at http://www.kakioka-jma.go.jp/obsdata/metadata/ja/products/2487/.

Kakioka Magnetic Observatory, 2015e, Memambetsu geomagnetic field 1-minute digital data in IAGA-2002 format, data set accessed 9 December 2016 at http://www.kakioka-jma.go.jp/obsdata/metadata/ja/products/2491/.

Kakioka Magnetic Observatory, 2015f, Memambetsu geomagnetic field 1-second digital data in IAGA-2002 format, data set accessed 17 June 2017 at http://www.kakioka-jma.go.jp/obsdata/metadata/ja/products/2493/.

Kakioka Magnetic Observatory, 2019, Digital data service, http://www.kakioka-jma.go.jp/obsdata/metadata/ja, Accessed 12 April 2019.

Mizunaga, H., 2016, Reduction of coherent noise from MT data using independent component analysis: Proceedings of the 134th SEGJ Conference, 154–156.

Mukai, R., H. Sawada, S. Araki, and S. Makino, 2003, Robust real-time blind source separation for moving speakers in a room: Proceedings of the IEEE International Conference on Acoustics, Speech, and Signal Processing, 469–472.

Murata, N., and S. Ikeda, 1998, An on-line algorithm for blind source separation on speech signals: Proceedings of the 9th International Symposium on Nonlinear Theory and Its Application, 923–926.

Murphy, B. S., and G. D. Egbert, 2018, Source biases in midlatitude magnetotelluric transfer functions due to Pc3-4 geomagnetic pulsations: Earth, Planets and Space, **70**, 12, doi: 10.1186/s40623-018-0781-0.

Neukirch, M., and X. Garcia, 2014, Nonstationary magnetotelluric data processing with instantaneous parameter: Journal of Geophysical Research, Solid Earth, **119**, 1634–1654, doi: 10.1002/2013JB010494.

Peacock, J. R., S. Thiel, G. S. Heinson, and P. Reid, 2013, Time-lapse magnetotelluric monitoring of an enhanced geothermal system: Geophysics, **78**, no. 3, B121–B130, doi: 10.1190/geo2012-0275.1.

Rees, N., S. Carter, G. Heinson, L. Krieger, D. Conway, G. Boren, and C. Matthews, 2016, Magnetotelluric monitoring of coal-seam gas and shale-gas resource development in Australia: The Leading Edge, **35**, 64–70, doi: 10.1190/tle35010064.1.

Romano, G., M. Balasco, V. Lapenna, A. Siniscalchi, L. Telesca, and S. Tripaldi, 2014, On the sensitivity of long-term magnetotelluric monitoring in Southern Italy and source-dependent robust single station transfer function variability: Geophysical Journal International, **197**, 1425–1441, doi: 10.1093/gji/ggu083.

Sato, S., T. Goto, T. Kasaya, K. Kawada, H. Iwamoto, and K. Kitada, 2017, Noise reduction method of marine spontaneous electric field data using independent component analysis: BUTSURITANSA (Geophysical Explorations), **70**, 42–55, doi: 10.3124/segj.70.42.

Sawada, H., S. Araki, R. Mukai, and S. Makino, 2006, Blind extraction of dominant target sources using ICA and time-frequency masking: IEEE Transactions on Audio, Speech, and Language Processing, **14**, 2165–2173, doi: 10.1109/TASL.2006.872599.

Sawada, H., R. Mukai, S. Araki, and S. Makino, 2003, Polar coordinate based nonlinear function for frequency-domain blind source separation: IEICE Transactions on Fundamentals of Electronics, Communications and Computer Sciences, **86**, 590–596, doi: 10.1109/ICASSP.2002.5743963.

Sawada, H., R. Mukai, S. Araki, and S. Makino, 2004, A robust and precise method for solving the permutation problem of frequency-domain blind source separation: IEEE Transactions on Speech and Audio Processing, **12**, 530–538, doi: 10.1109/TSA.2004.832994.

Smaragdis, P., 1998, Blind separation of convolved mixtures in the frequency domain: Neurocomputing, **22**, 21–34, doi: 10.1016/S0925-2312(98)00047-2.

Smirnov, M. Y., and G. D. Egbert, 2012, Robust principal component analysis of electromagnetic arrays with missing data: Geophysical Journal International, **190**, 1423–1438, doi: 10.1111/j.1365-246X.2012.05569.x.

Szarka, L., 1988, Geophysical aspects of man-made electromagnetic noise in the earth — A review: Surveys in Geophysics, **9**, 287–318, doi: 10.1007/BF01901627.

Tachibana, K., H. Saruwatari, Y. Mori, S. Miyabe, K. Shikano, and A. Tanaka, 2007, Efficient blind source separation combining closed-form second-order ICA and nonclosed-form higher-order ICA: Proceedings of the IEEE International Conference on Acoustics, Speech and Signal Processing, 71–74.

Tsuno, S., and Y. Iwata, 2015, Investigation of waveform separation by Independent Component Analysis for composite signals — As a target for mixed signals of earthquake ground motions and railway-induced ground vibrations: BUTSURITANSA (Geophysical Explorations), **68**, 39–47, doi: 10.3124/segj.68.39.

Vörös, Z., P. Kovács, A. Juhász, A. Körmendi, and A. W. Green, 1998, Scaling laws from geomagnetic time series: Geophysical Research Letters, **25**, 2621–2624, doi: 10.1029/98GL01910.

Vozoff, K., 1972, The magnetotelluric method in the exploration of sedimentary basins: Geophysics, **37**, 98–141, doi: 10.1190/1.1440255.

Weckmann, U., A. Magunia, and O. Ritter, 2005, Effective noise separation for magnetotelluric single site data processing using a frequency domain selection scheme: Geophysical Journal International, **161**, 635–652, doi: 10.1111/j.1365-246X.2005.02621.x.

Biographies and photographs of the authors are not available.